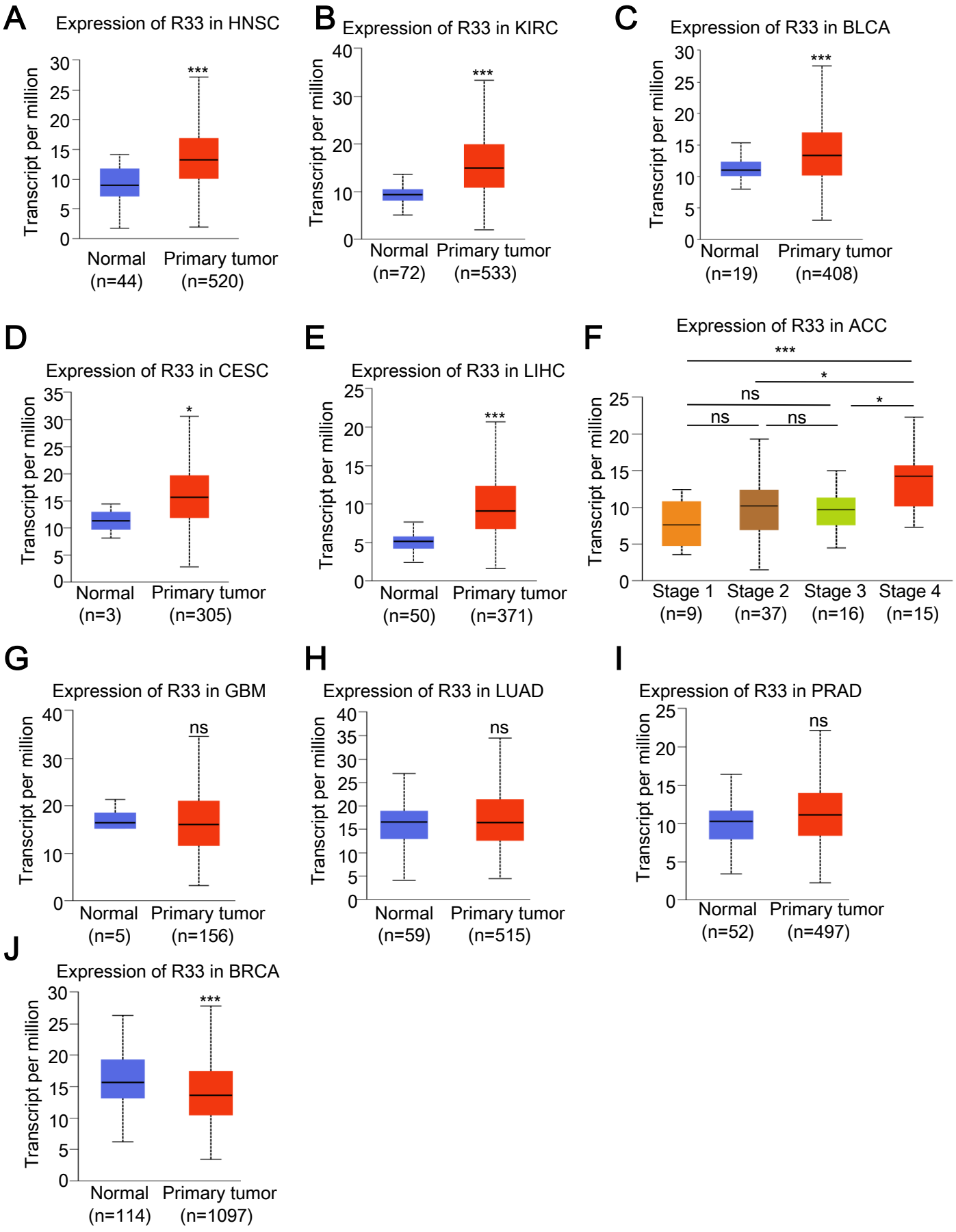

Figure S1. TCGA database analysis the expression of RBM33 in diverse solid tumors, related to Figure 1. Data shown as medians with SEM.

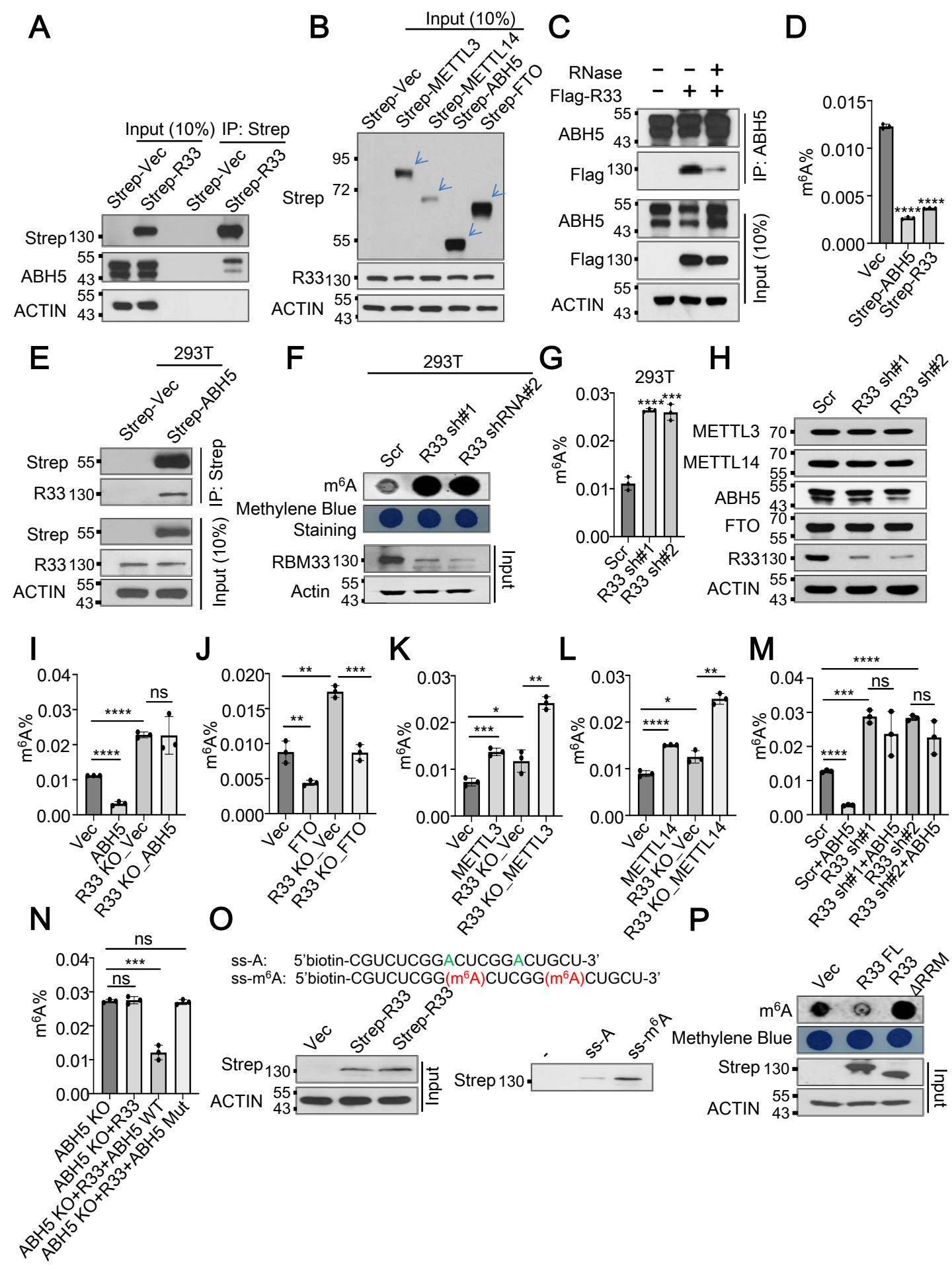
A
Input (10%)
IP: Strep
Strep-Vec
Strep-R33
Strep-Vec
Strep-R33
Strep 130
ABH5 55 43
ACTIN 55 43
B
Input (10%)
Strep-Vec
Strep-METTL3
Strep-METTL14
Strep-ABH5
Strep-FTO
95
72
55
Strep
R33 130
ACTIN 55 43
C
RNase − − +
Flag-R33 − + +
ABH5 55 43
Flag 130
IP: ABH5
ABH5 55 43
Flag 130
ACTIN 55 43
Input (10%)
D
m6A%
0.015
0.010
0.005
0.000
****
****
Vec
Strep-ABH5
Strep-R33
E
293T
Strep-Vec
Strep-ABH5
Strep 55
R33 130
IP: Strep
Strep 55
R33 130
ACTIN 55 43
Input (10%)
F
293T
Scr
R33 sh#1
R33 shRNA#2
m6A
Methylene Blue Staining
RBM33 130
Actin 55 43
Input
G
293T
m6A%
0.03
0.02
0.01
0.00
****
***
Scr
R33 sh#1
R33 sh#2
H
Scr
R33 sh#1
R33 sh#2
METTL3 70
METTL14 70 55
ABH5 55 43
FTO 70 55
R33 130
ACTIN 55 43
I
m6A%
0.04
0.03
0.02
0.01
0.00
****
****
ns
Vec
ABH5
R33 KO_Vec
R33 KO_ABH5
J
m6A%
0.020
0.015
0.010
0.005
0.000
**
**
***
Vec
FTO
R33 KO_Vec
R33 KO_FTO
K
m6A%
0.03
0.02
0.01
0.00
*
***
**
Vec
METTL3
R33 KO_Vec
R33 KO_METTL3
L
m6A%
0.03
0.02
0.01
0.00
*
****
**
Vec
METTL14
R33 KO_Vec
R33 KO_METTL14
M
m6A%
0.04
0.03
0.02
0.01
0.00
****
***
ns
ns
****
Scr
Scr+ABH5
R33 sh#1
R33 sh#1+ABH5
R33 sh#2
R33 sh#2+ABH5
N
m6A%
0.04
0.03
0.02
0.01
0.00
ns
***
ns
ABH5 KO
ABH5 KO+R33
ABH5 KO+R33+ABH5 WT
ABH5 KO+R33+ABH5 Mut
O
ss-A: 5'biotin-CGUCUCGGACUCGGACUGCU-3'
ss-m6A: 5'biotin-CGUCUCGG(m6A)CUCGG(m6A)CUGCU-3'
Vec
Strep-R33
Strep-R33
Strep 130
ACTIN 55 43
Input
ss-A
ss-m6A
Strep 130
P
Vec
R33 FL
R33 ΔRRM
m6A
Methylene Blue
Strep 130
ACTIN 55 43
Input

Figure S2 RBM33 depletion specifically inhibits ALKBH5 m^{6}A demethylase activity in UM-SCC-1 cells, related to Figure 1 and Figure 2. (A) Co-IP analysis suggests exogenous RBM33 associated with endogenous ALKBH5. Co-IP analysis was performed in UM-SCC-1 cells stably expressing strep-tagged vector, and strep-tagged RBM33 by using Step-Tactin beads. (B) Input of Fig. 1D. (C) The interaction between RBM33 and ALKBH5 relies on RNA substrate. (D) RNA m^{6}A methylation analysis suggests that RBM33 overexpression significantly inhibits global RNA m^{6}A methylation in UM-SCC-1 cells. Data shown as medians with SEM. (E) Co-IP analysis suggests RBM33 interacts with ALKBH5 in HEK293T cells. (F and G) RNA m^{6}A methylation analysis suggests that RBM33 knockdown significantly increases RNA m^{6}A methylation in HEK293T cells by dot-blot and RNA m^{6}A methylation quantification kit respectively. (H) Western blot analysis showing the effect of RBM33 knocking down on protein levels of m^{6}A writers and erasers in UM-SCC-1 cells. (I-L) RNA m^{6}A methylation analysis suggests that RBM33 knockdown selectively inhibits RNA m^{6}A demethylase ALKBH5 activity in UM-SCC-1 cells. Data shown as medians with SEM. (M) RNA m^{6}A methylation analysis suggests that RBM33 knockdown significantly inhibits ALKBH5 m^{6}A demethylase activity in UM-SCC-1 cells. Data shown as medians with SEM. (N) RNA m^{6}A methylation analysis showing the effect of ALKBH5 knockout on RBM33-mediated down-regulation of RNA m^{6}A methylation in HEK293T cells. Data shown as medians with SEM. (O) Exogenous RBM33 preferentially binds to m^{6}A-modfied RNA oligos. Substrate pull-down analyses suggest both exogenous and endogenous RBM33 preferentially bind to m^{6}A-modified RNA oligos. (P) Dot-blot analysis suggests that deletion RNA-recognition motif (RRM) of RBM33 blocks RBM33-mediated down-regulation of global RNA m^{6}A methylation.

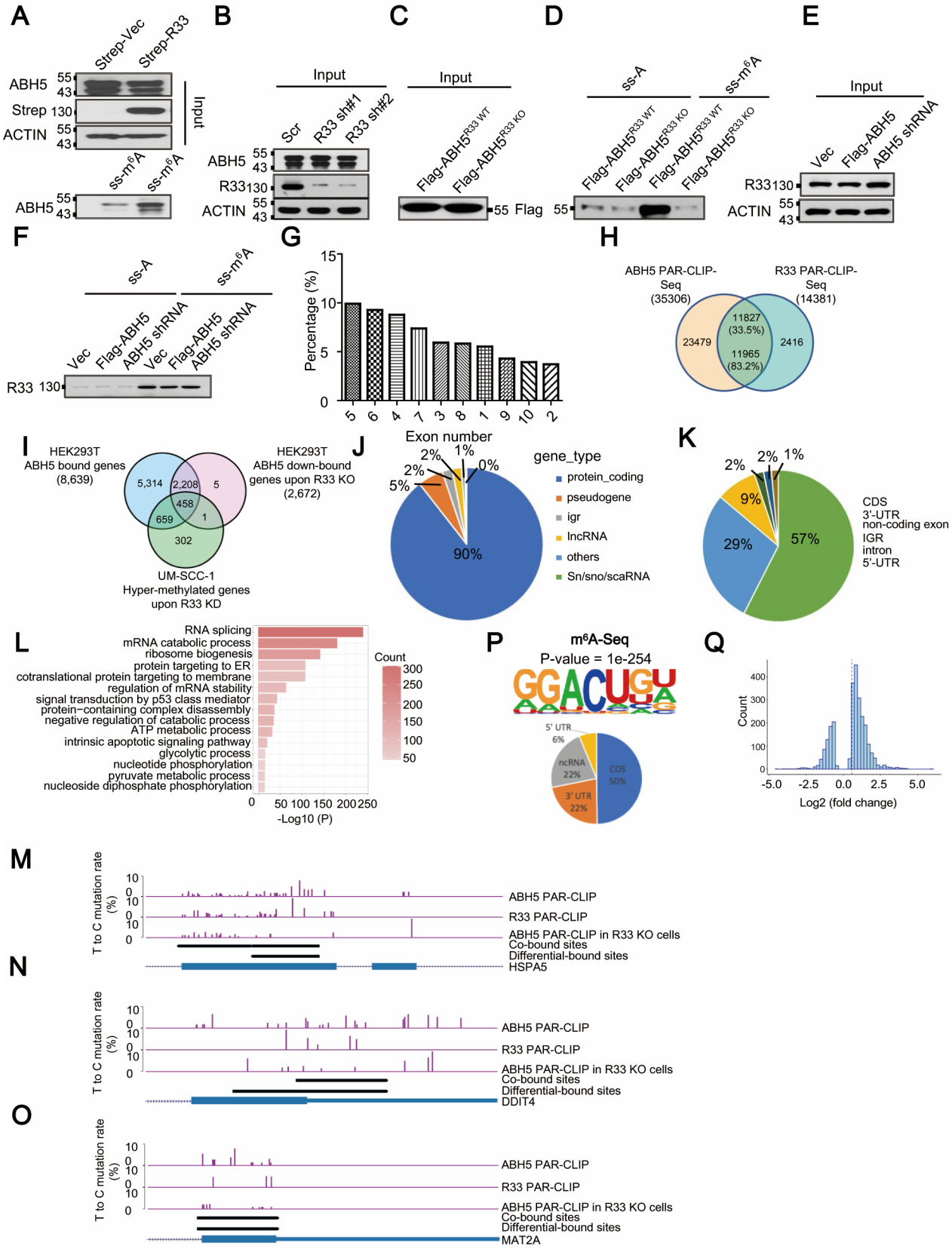
A
Strep-Vec
Strep-R33
ABH5
Strep
ACTIN
Input
ss-m6A
ss-m6A
ABH5
B
Input
Scr
R33 sh#1
R33 sh#2
ABH5
R33
ACTIN
C
Input
Flag-ABH5R33 WT
Flag-ABH5R33 KO
Flag
D
ss-A
ss-m6A
Flag-ABH5R33 WT
Flag-ABH5R33 KO
Flag-ABH5R33 WT
Flag-ABH5R33 KO
E
Input
Vec
Flag-ABH5
ABH5 shRNA
R33
ACTIN
F
ss-A
ss-m6A
Vec
Flag-ABH5
ABH5 shRNA
Vec
Flag-ABH5
ABH5 shRNA
R33
G
Percentage (%)
H
ABH5 PAR-CLIP-Seq (35306)
R33 PAR-CLIP-Seq (14381)
23479
11827 (33.5%)
11965 (83.2%)
2416
I
HEK293T ABH5 bound genes (8,639)
HEK293T ABH5 down-bound genes upon R33 KO (2,672)
UM-SCC-1 Hyper-methylated genes upon R33 KD
5,314
2,208
5
458
659
1
302
J
Exon number
gene_type
protein_coding
pseudogene
igr
lncRNA
others
Sn/sno/scaRNA
90%
5%
2%
2%
1%
0%
K
CDS
3'-UTR
non-coding exon
IGR
intron
5'-UTR
57%
29%
9%
2%
2%
1%
L
RNA splicing
mRNA catabolic process
ribosome biogenesis
protein targeting to ER
cotranslational protein targeting to membrane
regulation of mRNA stability
signal transduction by p53 class mediator
protein-containing complex disassembly
negative regulation of catabolic process
ATP metabolic process
intrinsic apoptotic signaling pathway
glycolytic process
nucleotide phosphorylation
pyruvate metabolic process
nucleoside diphosphate phosphorylation
Count
-Log10 (P)
P
m6A-Seq
P-value = 1e-254
5' UTR 6%
ncRNA 22%
CDS 50%
3' UTR 22%
Q
Count
Log2 (fold change)
M
T to C mutation rate (%)
ABH5 PAR-CLIP
R33 PAR-CLIP
ABH5 PAR-CLIP in R33 KO cells
Co-bound sites
Differential-bound sites
HSPA5
N
T to C mutation rate (%)
ABH5 PAR-CLIP
R33 PAR-CLIP
ABH5 PAR-CLIP in R33 KO cells
Co-bound sites
Differential-bound sites
DDIT4
O
T to C mutation rate (%)
ABH5 PAR-CLIP
R33 PAR-CLIP
ABH5 PAR-CLIP in R33 KO cells
Co-bound sites
Differential-bound sites
MAT2A

Figure S3 RBM33 binding sites are close to ALKBH5 binding sites, related to Figure 2. (A) m^6A-modified RNA substrate pull-down analysis suggests that RBM33 overexpression significantly facilitates ALKBH5 substrate accessibility. (B) Input of Figure 2E. (C) Western blot analysis showing protein levels of Flag-tagged ALKBH5 purified from wild-type and RBM33 knockout 293T cells. (D) m^6A-modified RNA substrate pull-down analysis suggests that RBM33 knockout significantly blocks ALKBH5 substrate accessibility. Flag-tagged ALKBH5 proteins purified from wild-type and RBM33 knockout 293T cells were subjected to RNA oligo pull-down analysis. (E and F) m^6A-modified RNA substrate pull-down analysis suggests that RBM33 m^6A-binding ability can not be regulated by ALKBH5. (G) Bar figure showing the exon content for RBM33 binding transcripts by RBM33 PAR-CLIP-seq analysis. (H) PAR-CLIP-seq analyses suggest that the majority of RBM33 binding sites could be overlapped with ALKBH5. (I) Overlap analysis for ALKBH5 bound genes, ALKBH5 down-bound genes upon RBM33 KO in 293T cells and hypermethylated genes upon RBM33 KD in UM-SCC-1 cells. (J) Pie charts show the distribution of the overlapped RBM33 and ALKBH5 PAR-CLIP-seq reads in RNA classes. (K) Pie charts show the distribution of the overlapped RBM33 PAR-CLIP peaks. (L) Gene ontology analysis for the co-bound genes by RBM33 and ALKBH5 via PAR-CLIP-seq analysis. (M-O) IGV browser tracks showing RBM33 and ALKBH5 PAR-CLIP reads in three selected representative genes in wild-type and RBM33 knockout HEK293T cells. (P) Consensus sequence motif identified after analysis of a common m^6A peaks from three replicates. (Q) Histogram showing that the majority of genes co-regulated by ALKBH5 and RBM33 exhibit an increased m^6A methylation in ALKBH5 depleted cells.

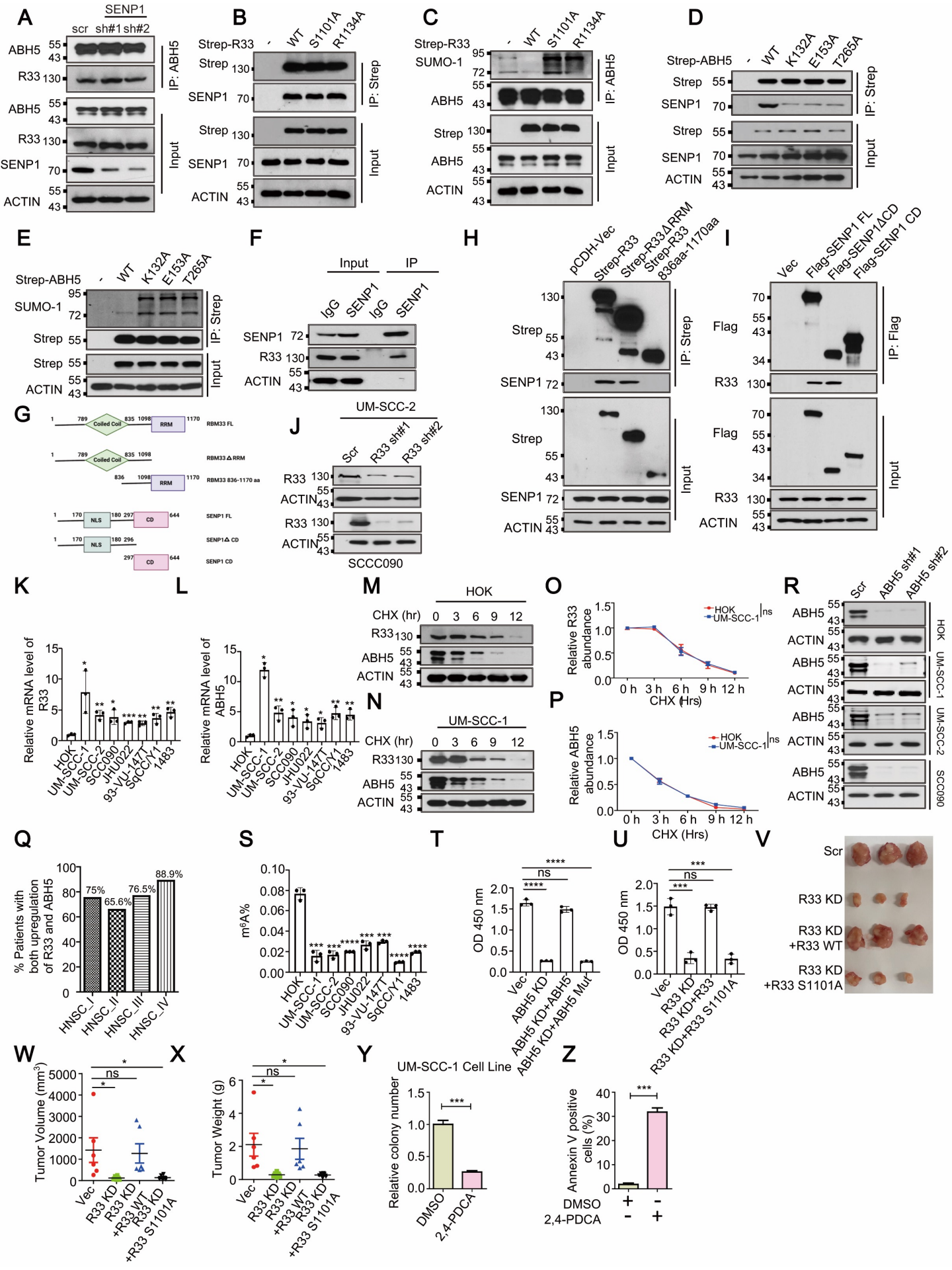
A
SENP1
scr sh#1 sh#2
ABH5
R33
IP: ABH5
Input
SENP1
ACTIN
B
Strep-R33
WT S1101A R1134A
Strep
SENP1
IP: Strep
Input
ACTIN
C
Strep-R33
SUMO-1
ABH5
IP: ABH5
Strep
Input
D
Strep-ABH5
WT K132A E153A T265A
IP: Strep
E
F
Input
IP
IgG SENP1 IgG SENP1
G
Coiled Coil
RRM
NLS
CD
RBM33 FL
RBM33 ΔRRM
RBM33 836-1170 aa
SENP1 FL
SENP1 ΔCD
SENP1 CD
H
pCDH-Vec
Strep-R33
Strep-R33 ΔRRM
Strep-R33 836aa-1170aa
I
Vec
Flag-SENP1 FL
Flag-SENP1 ΔCD
Flag-SENP1 CD
Flag
IP: Flag
J
UM-SCC-2
Scr
R33 sh#1
R33 sh#2
SCCC090
K
Relative mRNA level of R33
HOK
UM-SCC-1
UM-SCC-2
SCC090
JHU022
93-VU-147T
SqCC/Y1
1483
L
Relative mRNA level of ABH5
M
HOK
CHX (hr) 0 3 6 9 12
N
UM-SCC-1
O
Relative R33 abundance
CHX (Hrs)
ns
P
Relative ABH5 abundance
R
Scr
ABH5 sh#1
ABH5 sh#2
Q
% Patients with both upregulation of R33 and ABH5
75%
65.6%
76.5%
88.9%
HNSC_I
HNSC_II
HNSC_III
HNSC_IV
S
m⁶A%
T
OD 450 nm
Vec
ABH5 KD
ABH5 KD+ABH5
ABH5 KD+ABH5 Mut
U
Vec
R33 KD
R33 KD+R33
R33 KD+R33 S1101A
V
Scr
R33 KD
R33 KD +R33 WT
R33 KD +R33 S1101A
W
Tumor Volume (mm³)
Vec
R33 KD
R33 KD +R33 WT
R33 KD +R33 S1101A
X
Tumor Weight (g)
Y
UM-SCC-1 Cell Line
Relative colony number
DMSO
2,4-PDCA
Z
Annexin V positive cells (%)
DMSO
2,4-PDCA

Figure S4 RBM33/ALKBH5 complex regulates HNSCC cell survival in an m^{6}A dependent manner, related to Figure 4 and Figure 5. (A) Co-IP analysis suggests that the interaction between ALKBH5 and RBM33 can not be affected by KD of SENP1. (B) Co-IP analysis suggests that the interaction between RBM33 and SENP1 can not be affected by blocking the interaction between RBM33 and ALKBH5. (C) Denaturing IP assay suggests that SUMOylation of ALKBH5 can be extensively induced by overexpression of ALKBH5 interaction defective RBM33 mutant S1101A and R1134A. (D) Co-IP analysis suggests that the interaction between ALKBH5 and SENP1 can be significantly disrupted by blocking the interaction between RBM33 and ALKBH5. (E) Denaturing IP assay suggests that SUMOylation of ALKBH5 can be significantly induced by overexpression of RBM33 interaction defective mutant ALKBH5 K132A, E153A and T265A. (F) Co-IP analysis suggests that endogenous RBM33 interacts with endogenous SENP1. (G) Illustration of the regions for truncation mutants of both human RBM33 and ALKBH5. (H and I) Co-IP analyses suggest that the Coiled coil domain of RBM33 interacts with N-terminal of SENP1. (J) Western blot analysis showing the knockdown efficiency of RBM33 in UM-SCC-2 cells and SCC090 cells. (K and L) RT-qPCR analyses showing transcription levels of both RBM33 and ALKBH5 in normal control HOK cells and HNSCC cell lines. (M-P) Protein half-lives analyses for both RBM33 and ALKBH5 in normal control HOK cells and HNSCC cells. (Q) Immunohistochemical Staining (IHC) analysis suggests that RBM33 and ALKBH5 are simultaneously overexpressed in primary tumor tissues from different TNM stages of HNSC patients. In total, we analyzed 4 samples in stage I HNSCC TNM, 32 samples in stage II, 34 samples in stage III and 18 samples in stage IV. (R) Western blot analysis showing the knockdown efficiency of ALKBH5 in cell lines as indicated. (S) RNA m^{6}A methylation levels in normal control HOK cells, and HNSC cell line such as UM-SCC-1, UM-SCC-2, SCC090, JHU022, 93-VU-147T, SqCC/Y1 and 1483. Data shown as medians with SEM. (T) CCK8 analysis showing the effect of wild-type and enzymatic mutant ALKBH5 overexpression on ALKBH5 knockdown-mediated UM-SCC-1 cell proliferation inhibition. (U) CCK8 analysis showing the effect of wild-type and ALKBH5 interaction defective mutant RBM33 (RBM33 S1101A) overexpression on RBM33 knockdown-mediated UM-SCC-1 cell proliferation inhibition. (V-X) Effect of wild-type and ALKBH5 interaction-defective mutant RBM33 overexpression on RBM33 knockdown-mediated tumor growth inhibition of UM-SCC-1 xenograft. (Y) Colony forming analysis showing the colony forming ability of UM-SCC-1 cells with or without 2,4-PDCA treatment. Data shown as medians with SEM. (Z) Annexin V staining analysis showing the cell apoptosis of UM-SCC-1 cells with or without 2,4-PDCA treatment. Data shown as medians with SEM.

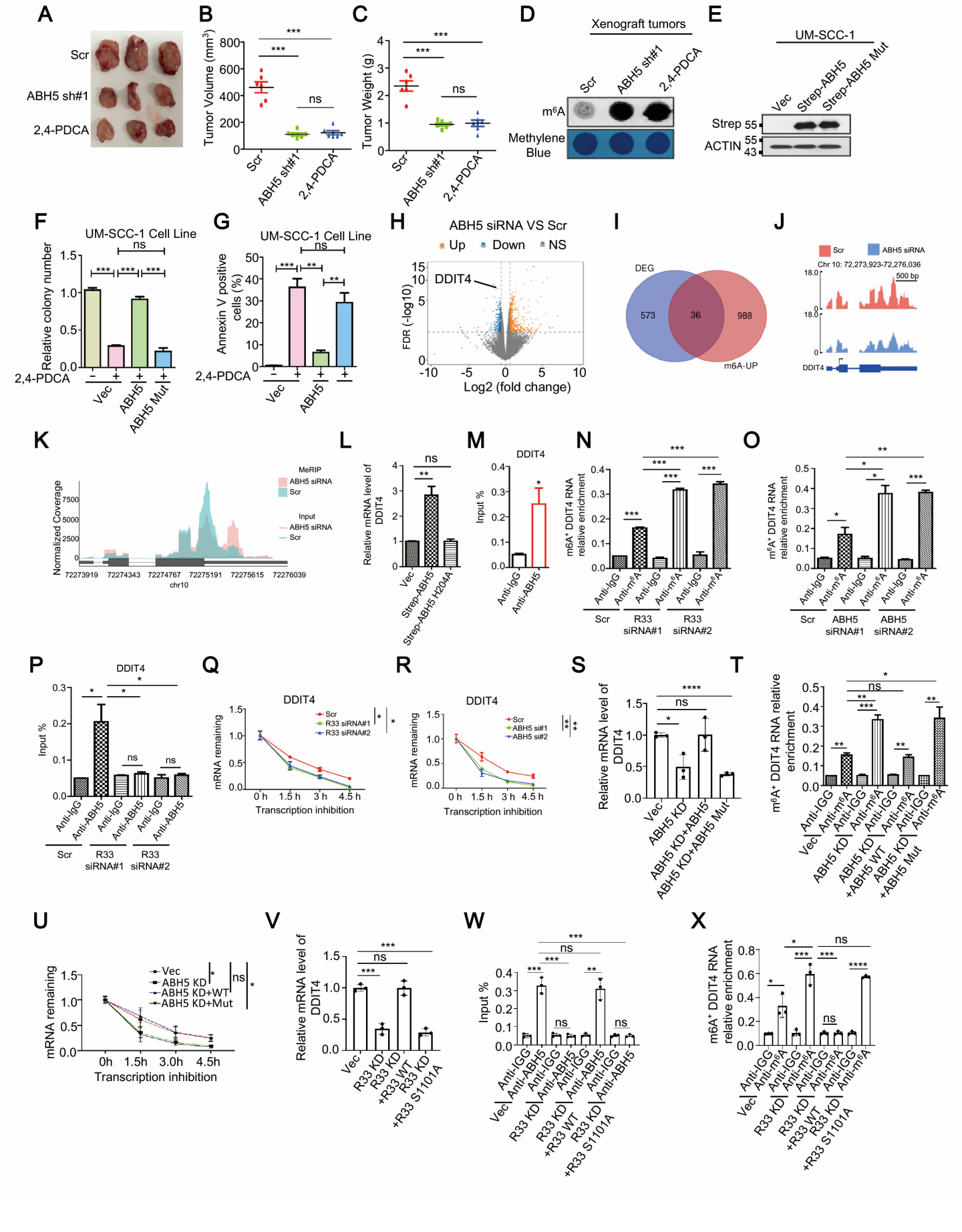
A
Scr
ABH5 sh#1
2,4-PDCA
B
Tumor Volume (mm3)
Scr
ABH5 sh#1
2,4-PDCA
C
Tumor Weight (g)
D
Xenograft tumors
m6A
Methylene Blue
E
UM-SCC-1
Vec
Strep-ABH5
Strep-ABH5 Mut
Strep
ACTIN
F
UM-SCC-1 Cell Line
Relative colony number
2,4-PDCA
Vec
ABH5
ABH5 Mut
G
UM-SCC-1 Cell Line
Annexin V positive cells (%)
H
ABH5 siRNA VS Scr
Up
Down
NS
DDIT4
FDR (-log10)
Log2 (fold change)
I
DEG
573
36
988
m6A-UP
J
Scr
ABH5 siRNA
Chr 10: 72,273,923-72,276,036
500 bp
DDIT4
K
MeRIP
ABH5 siRNA
Scr
Input
Normalized Coverage
chr10
L
Relative mRNA level of DDIT4
Vec
Strep-ABH5
Strep-ABH5 H204A
M
DDIT4
Input %
Anti-IgG
Anti-ABH5
N
m6A+ DDIT4 RNA relative enrichment
Anti-m6A
Scr
R33 siRNA#1
R33 siRNA#2
O
m6A+ DDIT4 RNA relative enrichment
ABH5 siRNA#1
ABH5 siRNA#2
P
DDIT4
Input %
Q
DDIT4
Scr
R33 siRNA#1
R33 siRNA#2
mRNA remaining
Transcription inhibition
R
DDIT4
ABH5 si#1
ABH5 si#2
S
Relative mRNA level of DDIT4
Vec
ABH5 KD
ABH5 KD+ABH5
ABH5 KD+ABH5 Mut
T
m6A+ DDIT4 RNA relative enrichment
Anti-IGG
Anti-m6A
ABH5 KD
+ABH5 WT
+ABH5 Mut
U
Vec
ABH5 KD
ABH5 KD+WT
ABH5 KD+Mut
mRNA remaining
Transcription inhibition
V
Relative mRNA level of DDIT4
R33 KD
+R33 WT
+R33 S1101A
W
Input %
X
m6A+ DDIT4 RNA relative enrichment

Figure S5 ALKBH5/RBM33 complex regulates gene expression of DDIT4 in an m^{6}A-dependent manner, related to Figure 5, Figure 6 and Figure 7. (A-C) Effect of ALKBH5 depletion or inhibition on UM-SCC-1 xenograft growth *in vivo*. Data shown as medians with SEM. (D) Dot blot analysis showing that ALKBH5 depletion or inhibition significantly increases global mRNA m^{6}A methylation *in vivo*. (E) Western blot analysis showing the protein expression of wild-type or enzymatic mutant ALKBH5 (ALKBH5 H204A). (F) Colony formation analysis showing that 2,4-PDCA-mediated inhibitory effect on UM-SCC-1 colony forming ability could be rescued by wild-type but not enzymatic mutant ALKBH5 overexpression. Data shown as medians with SEM. (G) Annexin V staining analysis showing the 2,4-PDCA-induced UM-SCC-1 cells apoptosis could be rescued by the wild-type but not enzymatic mutant ALKBH5 overexpression. Data shown as medians with SEM. (H) ALKBH5 knockdown leads to significant gene expression alterations. Differentially expressed genes shown in volcano figure in control or ALKBH5-depleted samples. (I) The Venn diagram shows a number of genes with both significant m^{6}A increase and differential expression upon RBM33 and ALKBH5 knockdown. (J) RNA-Seq peak visualization of DDIT4 in control and ALKBH5-depleted cells. (K) m^{6}A peak visualization of DDIT4 in control and ALKBH5-depleted cells. (L) RT-qPCR analysis showing the effect of ALKBH5 overexpression on transcripts of DDIT4 in UM-SCC-1 cells. (M) ALKBH5 RIP analysis suggests that ALKBH5 directly binds to transcripts of DDIT4 in UM-SCC-1 cells. Data shown as medians with SEM. (N and O) MeRIP analysis suggests that either RBM33 or ALKBH5 depletion significantly increases DDIT4 mRNA m^{6}A methylation. Data shown as medians with SEM. (P) ALKBH5 RIP analysis suggests that ALKBH5 enrichment at DDIT4 transcripts could be blocked by RBM33 KD. Data shown as medians with SEM. (Q) mRNA half-life analysis indicates that RBM33 KD significantly promotes mRNA decay of DDIT4. Data shown as medians with SEM. (R) mRNA half-life analysis suggests that ALKBH5 depletion significantly promotes mRNA decay of DDIT4. Data shown as medians with SEM. (S) RT-qPCR analysis showing the effect of wild-type and enzymatic mutant ALKBH5 (ALKBH5 H204A) overexpression on ALKBH5 knockdown-mediated down-regulation of DDIT4. Data shown as medians with SEM. (T) MeRIP analysis suggests that ALKBH5 depletion-induced up-regulation of DDIT4 mRNA m^{6}A methylation can be rescued by wild-type ALKBH5 overexpression. Data shown as medians with SEM. (U) mRNA half-life analysis suggests that ALKBH5 depletion-induced mRNA decay of DDIT4 can be rescued by wild-type but not enzymatic mutant ALKBH5 overexpression. Data shown as medians with SEM. (V) RT-qPCR analysis showing the effect of wild-type and ALKBH5 interaction defective mutant RBM33 (RBM33 S1101A) overexpression on RBM33 knockdown-mediated down-regulation of DDIT4. Data shown as medians with SEM. (W) ALKBH5 RIP analysis suggests that only wild-type RBM33 overexpression can rescue the decreased ALKBH5 enrichment at DDIT4 transcripts mediated by RBM33 knockdown. Data shown as medians with SEM. (X) MeRIP analysis suggests that RBM33 depletion induced up-regulation of DDIT4 mRNA m^{6}A methylation can be rescued by wild-type but not ALKBH5 interaction defective mutant RBM33 overexpression. Data shown as medians with SEM.

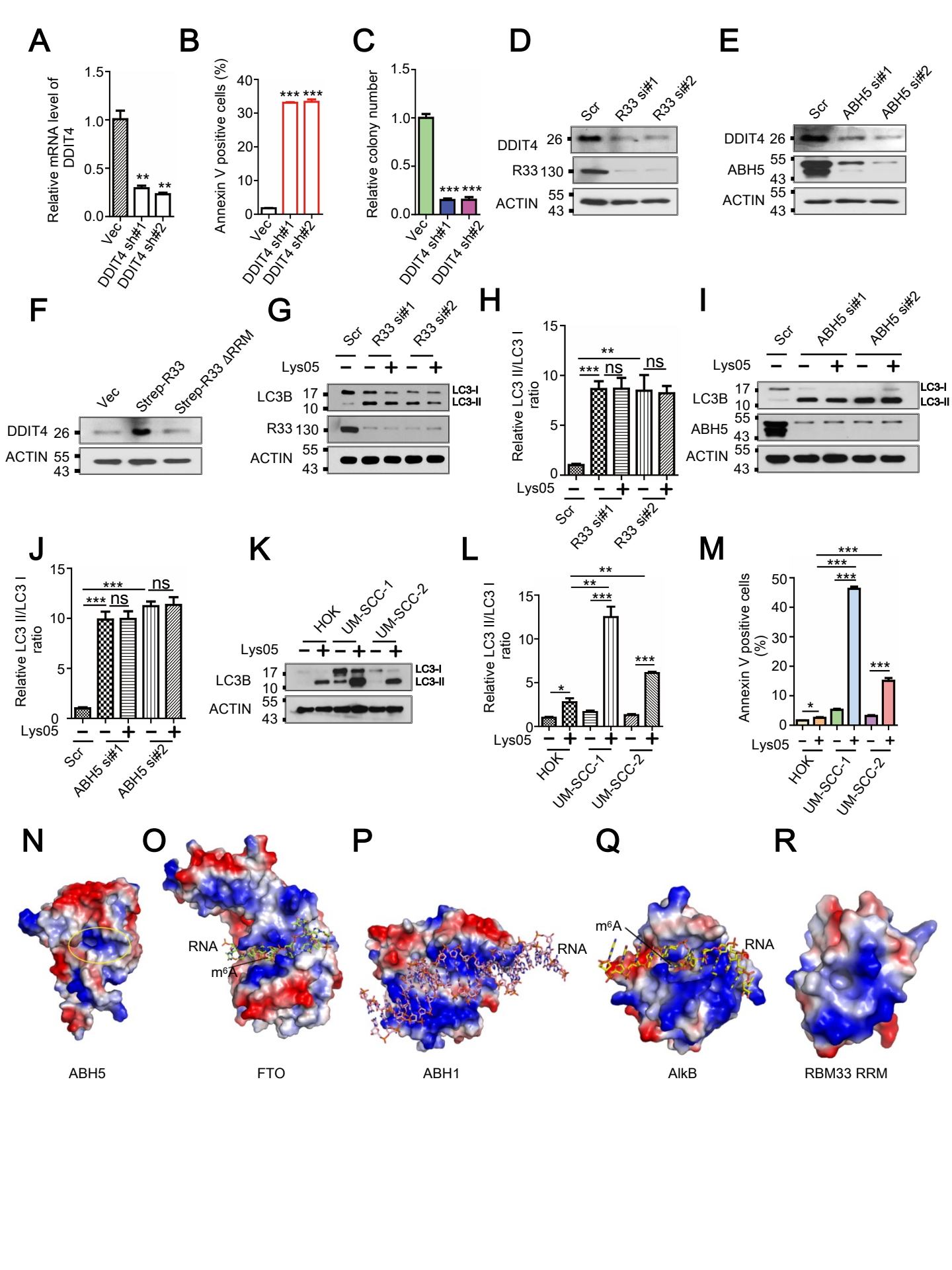
A
Relative mRNA level of DDIT4
Vec
DDIT4 sh#1
DDIT4 sh#2
B
Annexin V positive cells (%)
C
Relative colony number
D
Scr
R33 si#1
R33 si#2
DDIT4
R33
ACTIN
E
Scr
ABH5 si#1
ABH5 si#2
DDIT4
ABH5
ACTIN
F
Vec
Strep-R33
Strep-R33 ΔRRM
DDIT4
ACTIN
G
Scr
R33 si#1
R33 si#2
Lys05
LC3B
LC3-I
LC3-II
R33
ACTIN
H
Relative LC3 II/LC3 I ratio
ns
Lys05
I
Scr
ABH5 si#1
ABH5 si#2
Lys05
LC3B
ABH5
ACTIN
J
Relative LC3 II/LC3 I ratio
ns
Lys05
Scr
ABH5 si#1
ABH5 si#2
K
HOK
UM-SCC-1
UM-SCC-2
Lys05
LC3B
ACTIN
L
Relative LC3 II/LC3 I ratio
Lys05
HOK
UM-SCC-1
UM-SCC-2
M
Annexin V positive cells (%)
Lys05
HOK
UM-SCC-1
UM-SCC-2
N
ABH5
O
RNA
m6A
FTO
P
RNA
ABH1
Q
m6A
RNA
AlkB
R
RBM33 RRM

Figure S6 HNSCC cells are more sensitive to autophagy inhibitor treatment as compared to the normal control HOK cells, related to Figure 7 and discussion section. (A) qRT-PCR analysis showing the KD efficiency of DDIT4 in UM-SCC-1 cells. Data shown as medians with SEM. (B) Annexin V staining analysis showing the effect of DDIT4 KD on cell apoptosis of UM-SCC-1. Data shown as medians with SEM. (C) Colony-forming analysis showing the effect of DDIT4 KD on colony-forming ability of UM-SCC-1. Data shown as medians with SEM. (D and E) Western blot analysis showing the effect of RBM33 (D) or ALKBH5 depletion (E) on protein levels of DDIT4 in UM-SCC-1 cells. (F) Western blot analysis showing the effect of wild-type and RBM33 depleting RRM domain overexpression on protein levels of DDIT4 in UM-SCC-1 cells. (G-J) Either RBM33 or ALKBH5 depletion significantly inhibits autophagy in UM-SCC-1 cells. Data shown as medians with SEM.
(K-L)Western blot analysis showing the effect of autophagy inhibitor treatment on protein levels of LC3B in the cell lines as indicated. Data shown as medians with SEM. (M) Cell apoptosis analysis showing that HNSC cells, UM-SCC-1 and UM-SCC-2 are more sensitive to autophagy inhibitor-induced cell apoptosis than the normal control HOK cells. Data shown as medians with SEM. (N-R) Comparison of electrostatic surfaces among ALKBH5, FTO, ALKBH1 and AlkB. Positively charged surface is colored in *blue*, negatively charged surface is colored in *red*, and neutral surface is colored in *white*. Alkbh5 (PDB 4O7X) is less positively charged compared with FTO (PDB 5ZMD), ALKBH1 (PDB 6KSF) and AlkB (PDB 4NID). The active center is shown in a *yellow ellipse*.

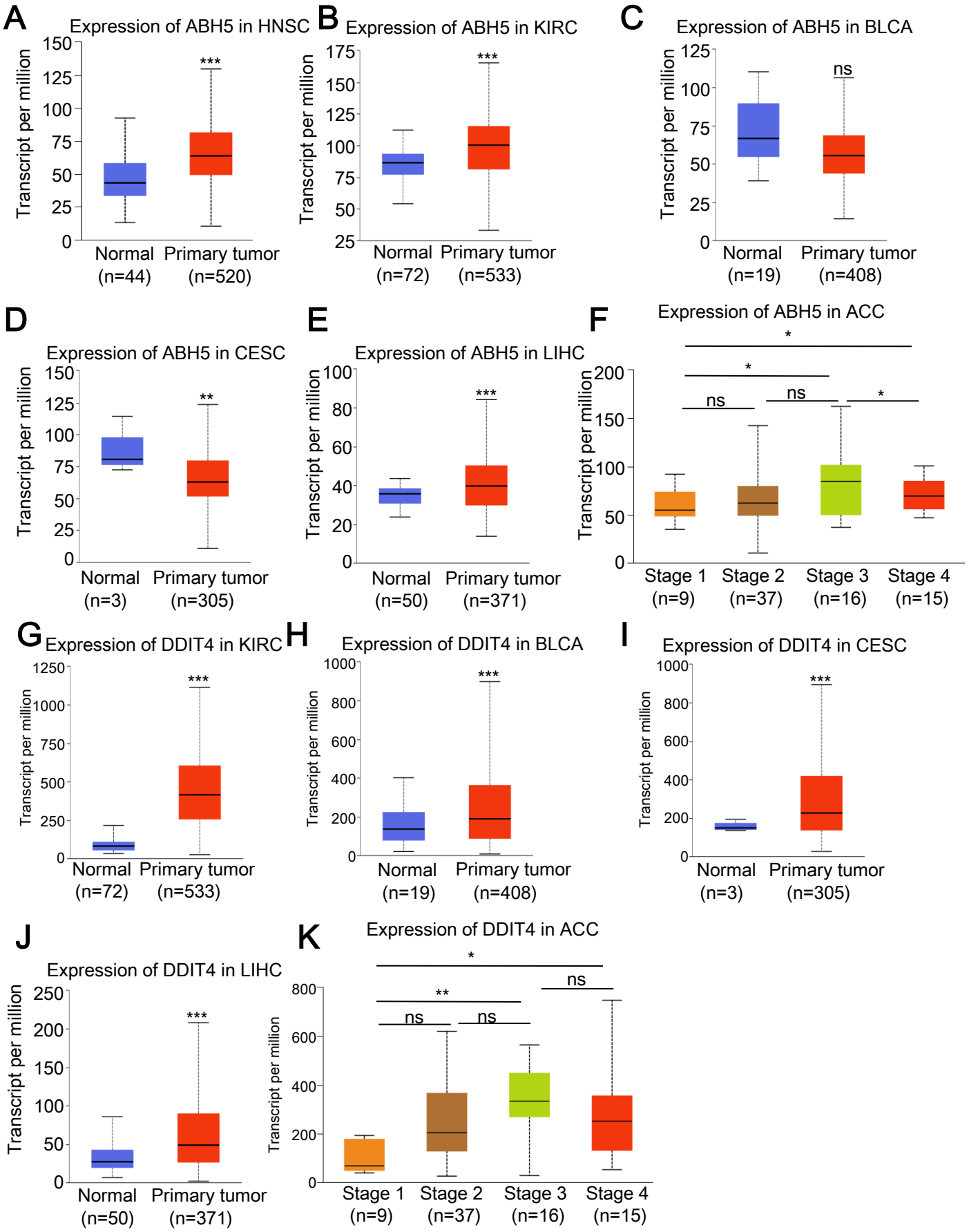

Figure S7 TCGA database analysis the expression of ALKBH5 and DDIT4 in RBM33 overexpressed solid tumors, related to Figure 7 and discussion section. Data shown as medians with SEM.